Research Square

Preprints are preliminary reports that have not undergone peer review.
They should not be considered conclusive, used to inform clinical practice,
or referenced by the media as validated information.

An Experimental Method for Simulating Reservoir Productivity Following Phase-Change Self-Propping Fracturing via Coupled Core Flooding and Fracture Conductivity Testing

Yuxin Pei

pyx121@126.com

Changzhou University

Anze Tang

Changzhou University

Feiting Luo

Changzhou University

Xikun Shan

Changzhou University

Yitao Chen

Changzhou University

Yufan Chen

Changzhou University

Research Article

Keywords: phase-change self-propping fracturing fluid, core flooding, fracture conductivity, matrix-fracture coupling, productivity prediction, unconventional reservoirs

Posted Date: November 25th, 2026

DOI: https://doi.org/10.21203/rs.3.rs-11737324/v1

License: This work is licensed under a Creative Commons Attribution 4.0 International License.
Read Full License

Additional Declarations: No competing interests reported.

An Experimental Method for Simulating Reservoir Productivity Following Phase-Change Self-Propping Fracturing via Coupled Core Flooding and Fracture Conductivity Testing

Yuxin Pei[a,b,*], Anze Tang[a], Feiting Luo[a], Xikun Shan[a], Yitao Chen[a], Yufan Chen[a]

a Changzhou University, Changzhou 213164, China;

b KeShengGao Energy Technology (Changzhou) Co., Ltd., Changzhou 213161, China

* Correspondence: pyx121@126.com

Abstract: To address the lack of methods for quantitative evaluation of dynamic conductivity and productivity of phase-change self-propping fracturing fluids under "matrix-fracture" coupled conditions, a series-coupled experimental apparatus combining core flooding and fracture conductivity testing was developed. Using cores with permeability ranges of 0.1–1 mD, 1–10 mD, and 10–20 mD, the reservoir damage, fracture conductivity, and productivity characteristics of broken slickwater systems (at concentrations of 1%, 2%, 6%, and 8%) carrying different proppants versus the phase-change self-propping fracturing fluid system were comparatively evaluated at 80 under closure pressures of 20–50 MPa. Furthermore, a quantitative workflow for predicting field productivity from laboratory conductivity experiments was established in combination with an equivalent wellbore radius model. The results show that the phase-change self-propping fracturing fluid forms uniform solid proppant particles in situ on the core end face which undergo only slight deformation under 50 MPa and exhibit excellent load-bearing integrity and low reservoir damage. The stimulated productivity declines slowly with increasing closure pressure. Across cores with varying permeability levels, the predicted productivity using this system is 1.3–1.6 times that of two proppant-laden broken slickwater systems (low-viscosity slickwater carrying quartz sand and high-viscosity slickwater carrying ceramic proppant). Furthermore, the 1% slickwater system exhibits a more pronounced stimulation advantage in high-permeability cores, and greater adaptability in medium-to-low permeability cores. The post-fracturing daily oil production of the field pilot well stabilized at 2–3 t, verifying the reliability of the productivity predictions obtained from the coupled experiment. This coupled experimental method provides an experimental basis and a productivity prediction tool for optimizing field operational parameters and promoting the large-scale application of phase-change self-propping fracturing fluids.

Keywords: phase-change self-propping fracturing fluid; core flooding; fracture conductivity; matrix-fracture coupling; productivity prediction; unconventional reservoirs

Introduction

With the continuous growth of global energy demand and the widening supply gap of conventional oil and gas resources, unconventional resources such as shale, tight sandstone, and coal seams have become vital replacement resources for increasing hydrocarbon reserves and production and safeguarding energy security in China [1,2]. Such reservoirs generally feature complex geological characteristics,

including low porosity, low permeability, low pore pressure, strong heterogeneity, well-developed natural fractures, and high in-situ stress. Some reservoirs also face challenges such as high temperature, high salinity, strong water sensitivity, and fracturing fluid flowback after fracturing. Among these problems, the flowback of fracturing fluid directly restricts the benefits in the development of unconventional oil and gas reservoirs [3,4]. Hydraulic fracturing serves as the cornerstone technology for achieving effective stimulation and commercial-scale development in such reservoirs [5]. As China has stepped up exploration and development of deep and ultra-deep unconventional resources in recent years, increasingly harsh downhole conditions have placed greater demands on fracturing fluids. They must withstand high temperatures and salinity, minimize leak-off and formation damage, break gel in a controlled manner, and support long-term fracture conductivity while preserving the integrity of the fracture network. [6–9].

Conventional proppant-carrying hydraulic fracturing mainly relies on two mainstream technologies: guar-based fracturing and slickwater fracturing. Guar-based fracturing fluids rely on crosslinking to form high-viscosity systems that suspend and transport proppants with low leak-off and strong carrying capability. However, their polymer chains are prone to scission and thermal degradation at elevated temperatures, generating substantial insoluble residues upon gel breaking; this induces severe fracture conductivity impairment under specific operating conditions and damages matrix permeability during flowback [10]. Slickwater offers the advantages of low viscosity, high drag reduction, and the capability to create complex fracture networks under high injection rates. Nevertheless, its extremely low base viscosity results in poor proppant transport, hindering proppant placement into secondary microfractures and fracture tips; furthermore, high-density proppants fail to prop these distal fractures effectively, ultimately impairing hydrocarbon recovery [11]. Both systems operate by carrying ex-situ solid proppants into fractures, which commonly causes issues such as proppant settling, discontinuous propping across the fracture network, and proppant crushing and flowback under high closure stress, resulting in severe formation damage and insufficient long-term conductivity [12,13]. Although novel materials such as variable-viscosity slickwater, supramolecular fracturing fluids, and thermally expandable smart proppants, as well as new techniques, have demonstrated advances in drag reduction, proppant transport, formation protection, and sustained fracture propping, limitations remain. These include high operational costs, narrow reservoir applicability, and inadequate propping across the full fracture network, which fail to fully satisfy the stimulation demands of complex unconventional reservoirs [14,15].

Furthermore, low-temperature gel breaking and the resulting formation damage potential are critical factors governing stimulation effectiveness. Incomplete gel breaking at low temperatures readily leads to fracturing fluid retention, forming filter cakes or gel-breaking residues that clog pore throats and diminish matrix permeability and fracture conductivity. Moreover, excessive residues with unfavorable particle size distributions further exacerbate formation damage—a challenge to which low-permeability

and tight reservoirs are particularly vulnerable[16]. Consequently, the formulation of fracturing fluid systems must balance controllable low-temperature gel breaking with minimal reservoir damage to improve flowback efficiency and preserve long-term fracture conductivity.

To overcome these technical bottlenecks, Chinese universities [17] and oilfield enterprises have collaboratively developed a phase-change self-propping fracturing fluid technology, achieving a fundamental transition from "ex-situ proppant transport" to "in-situ proppant generation." Throughout the fracturing operation, this technology pumps solely two liquid phases—a phase-change liquid (PCL) and a non-phase-change liquid (NPCL)—without injecting any solid particles into the wellbore. Under reservoir conditions, the PCL solidifies in situ to form proppant particles within the fracture. The NPCL remains liquid and flows back, leaving channels between the solidified particles for hydrocarbons to pass through. This approach avoids common challenges such as proppant settling, screenout, and proppant flowback [18]. In terms of fluid performance, this system exhibits low leak-off, minimal residues, and low reservoir damage, delivering a high core permeability recovery rate. The in-situ generated proppant particles exhibit excellent sphericity and high crush resistance, spanning mesh sizes from 6 to 300 mesh. Under high closure stress, their conductivity surpasses that of quartz sand and approaches that of ceramic proppants under certain conditions, enabling effective propping across primary fractures, secondary microfractures, and distal fracture tips [19,20]. In addition, by controlling shear conditions and optimizing the chemical formulations of dispersants and regulators, the system allows flexible tuning of proppant grain size, phase-change induction time, and transition temperature, thereby accommodating the stimulation design requirements of diverse reservoirs.

Given these material advantages, this phase-change self-propping fracturing fluid technology has undergone field pilot trials across multiple blocks, including the Changqing, Yanchang, and Huabei Oilfields. Notably, pilot well N1 in the Huabei Oilfield confirmed that the phase-change fluid solidifies in situ downhole to sustain fracture conductivity; virtually no solid proppant grains were produced in the flowback fluid, demonstrating effective proppant placement and retention within the fracture network [21]. Pilot wells Y156X and H61X in the Ordos Basin tight gas field of Changqing Oilfield were treated with this hybrid fracturing method. Although the resulting proppant packs had only one-third to one-half the strength of those in conventional treatments, well productivity matched or exceeded conventional results. Several treated wells also produced substantially more than conventionally fractured offset wells [22]. Similarly, in the Shaximiao tight gas reservoir of the Southwest Oil and Gas Field, pilot well 33X outperformed offset wells in daily gas production under identical stimulation scale, perforation intervals, and production regimes, demonstrating remarkable stimulation efficacy [23–26]. Although these pilot trials achieved encouraging stimulation results, field performance in unconventional reservoirs is inevitably complicated by multiple factors, such as reservoir heterogeneity, hydrocarbon richness, operational parameters, and production regimes. Due to the limited number of field cases, inter-well production comparisons alone cannot decouple these multivariable interferences

or elucidate the intrinsic stimulation mechanisms of this phase-change fracturing fluid system [27–31]. However, existing fracture conductivity evaluations are predominantly conducted under static closure stress without continuous fluid flow representative of long-term production. Consequently, they fail to capture the dynamic conductivity variations induced by proppant rearrangement and packing-structure evolution under fluid flushing [32]. Currently, the quantitative relationships among matrix damage, dynamic fracture conductivity, and reservoir productivity stimulated by phase-change self-propping fluids remain unclear; furthermore, experimental apparatus capable of simulating matrix–fracture coupled flow are still lacking. To address these challenges, this study establishes an experimental method to simulate post-fracturing reservoir productivity using a custom-developed apparatus that series-couples core flooding and fracture conductivity testing. This setup achieves full-process laboratory simulation of pumping, dispersion, in-situ phase transition, and hydrocarbon production for phase-change self-propping fluids. Through comparative tests with conventional proppant-transport fracturing systems, the long-term fracture conductivity retention and productivity characteristics are quantitatively evaluated, providing a novel experimental protocol and empirical foundation for parameter optimization and field-scale application.

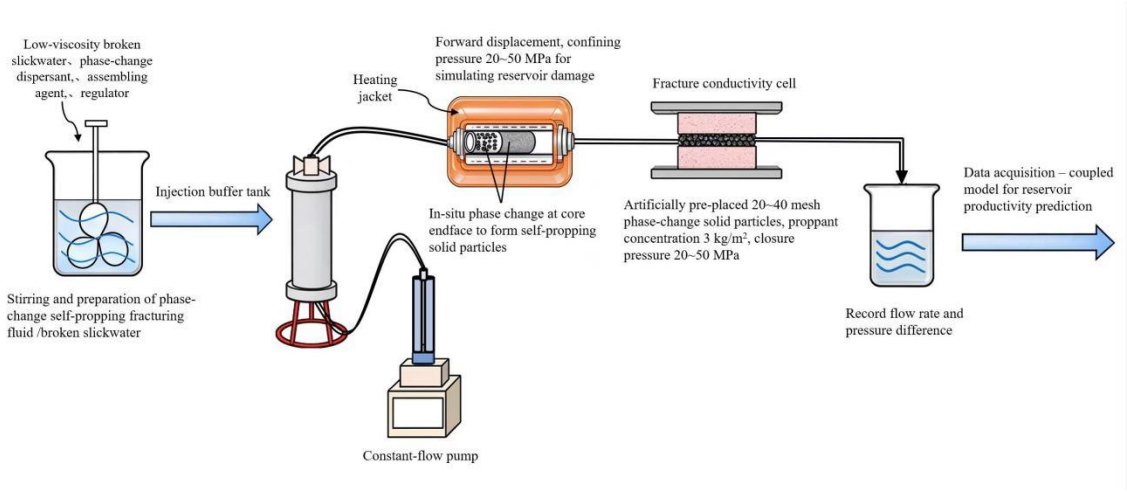

Fig. 1 Graphical abstract

1 Experimental Apparatus and Method

1.1 Experimental Apparatus

This study employed a self-developed experimental apparatus that connects a core flooding system in series with a fracture conductivity system. The apparatus consists of six functional systems: a pumping system, a confining pressure loading system, a temperature control system, a hydraulic loading system, a fracture conductivity system, and a data acquisition system. Together, they simulate the full process of pumping, dispersion, phase change, and production, as depicted in Fig. 2.

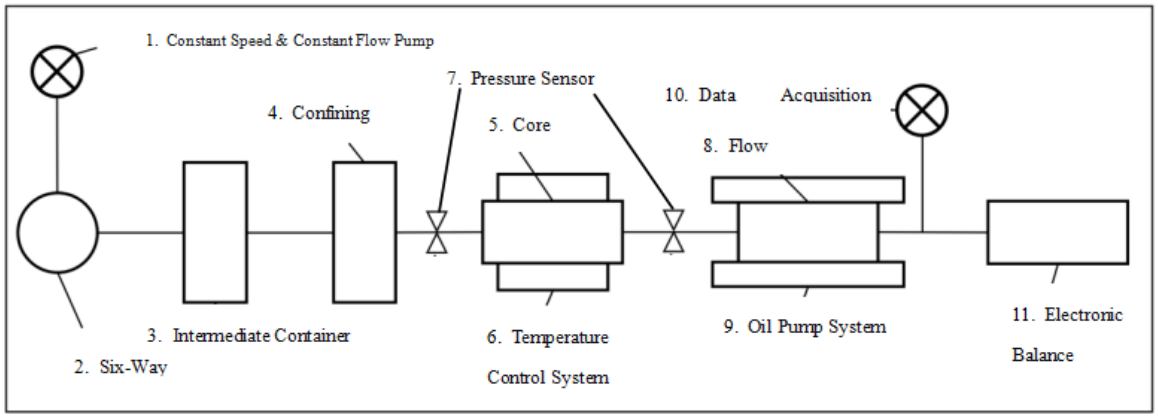



Fig. 2 Schematic diagram of the coupled core flooding and fracture conductivity apparatus

(1) The pumping system primarily consists of a constant-rate constant-pressure pump, a six-way valve, transfer cylinders, and flow lines. It accurately regulates pumping flow rate and pressure, achieves seamless fluid switching via the six-way valve, and injects fracturing fluid or diesel from the transfer cylinders into the core at a constant rate, accurately reproducing field pump rates and displacement processes.

(2) The confining pressure loading system is composed mainly of an automatic confining pressure tracking pump and a core holder. It applies annular confining pressure to the core holder to simulate overburden stress, ensuring tight sealing around the core periphery, replicating the realistic downhole tri-axial stress state, and preventing fluid channeling under elevated pressures.

(3) The temperature control system includes heating jackets, high-precision temperature sensors, and an intelligent temperature control unit. Wrapped around the core holder and conductivity cell, this system uniformly heats the apparatus to replicate target reservoir temperatures, ensuring that the phase-change self-propping fracturing fluid completes its phase change or gel-breaking reaction under downhole thermal conditions.

(4) The hydraulic loading system consists of a hydraulic oil pump, a loading piston, and a load-bearing frame. It exerts vertical closure stress on the fracture conductivity cell to simulate the variable closure stresses acting on fractures in situ, thereby evaluating proppant conductivity under the stresses.

(5) The fracture conductivity system is centered around an HTHP fracture conductivity cell. It allows in-situ generated solid proppant particles or conventional proppants to be packed at specified proppant areal concentrations to simulate post-fracture hydraulic fractures. Working in conjunction with the hydraulic loading system, it dynamically evaluates fracture aperture and conductivity across varying closure stresses.

(6) The data acquisition system is composed of high-precision pressure transducers, temperature sensors, flow meters, an electronic balance, and automated data acquisition software. It monitors and logs key real-time parameters throughout the test—including core holder inlet pressure, conductivity cell outlet pressure, differential pressure, flow rate, fluid temperature, and effluent mass—providing robust experimental data for subsequent productivity calculations and formation damage evaluations.

1.2 Experimental Method

1.2.1 Experimental Preparation and Material Formulation

Prior to testing, core plugs were vacuum-saturated with a 2% KCl brine, followed by initial permeability measurements to mitigate matrix damage induced by clay hydration. Vinyl monomers, acrylate monomers, unsaturated polyester resin, and a curing agent were proportioned and blended into a homogeneous resin mixture. Under continuous mechanical agitation, the mixture was dispersed into an aqueous phase containing a surfactant dispersant; by regulating stirring speed and dispersant concentration, the resin mixture was emulsified into spherical droplets spanning 6–300 mesh. A phase-change regulator was subsequently added to yield the final phase-change self-propping fracturing fluid.

To replicate the downhole shearing experienced during field pumping, the formulated phase-change fluid was sheared at high speeds to produce uniform micro-droplets and then injected across the face of the core holder at a water-to-base fluid volumetric ratio of 1:10. At an elevated temperature of 80 ° C, the fluid underwent an in-situ liquid-to-solid phase transition, generating a highly permeable pack of solid proppant particles across the core end face.

A 35% active-content suspension friction reducer was diluted to prepare 1‰ and 2‰ broken slickwater systems for carrying 20 – 40 mesh quartz sand, and 6‰ and 8‰ systems for carrying 20 – 40 mesh ceramic proppant; both benchmark systems were evaluated for fracture propping and simulation of post-fracture productivity.

1.2.2 Experimental Procedure for the Coupled Core Flooding and Fracture Conductivity System

The experiment utilized a series-coupled core flooding and fracture conductivity apparatus to simulate the complete production flow path: fluid flowing from the reservoir matrix into hydraulic fractures, then through the fractures to the wellbore.

First, oven-dried and weighed core plugs were mounted in the core holder. In-situ generated 20 – 40 mesh solid particles were then uniformly distributed inside the fracture conductivity cell at a target

proppant areal concentration of 3 kg/m² . For the broken slickwater systems, 20 – 40 mesh quartz sand and ceramic proppants were packed into the cell, respectively. Subsequently, the confining pressure loading and temperature control systems were engaged to bring both the core holder and conductivity cell to target downhole conditions (temperature: 80 ° C; confining pressure: 20 – 50 MPa), replicating the real tri-axial stress and thermal regime. The constant-pressure constant-rate pump was then started to inject 1% or 2% broken slickwater, or the phase-change self-propping fracturing fluid, from the transfer cylinders into the core plug at a constant rate for 10 pore volumes (PV) to induce formation damage. Following the damage phase, the effluent outlet of the core holder was connected to the inlet of the fracture conductivity cell. To evaluate variable reservoir stress regimes, the closure stress on the conductivity cell was incrementally adjusted to 20, 30, 40, and 50 MPa. Finally, counter-current flooding was initiated with diesel at a constant rate of 2.5 mL/min to simulate steady-state oil production. Once the effluent flow stabilized at the system discharge, differential pressure and flow rate were logged to calculate productivity under each condition.

1.2.3 Data Acquisition and Productivity Evaluation Model

Throughout the experimental sequence, the data acquisition system recorded real-time key parameters, including core holder inlet pressure, line pressure, conductivity cell outlet pressure, pump rate, discharge flow rate, and fluid temperature; effluent mass was continuously monitored using an electronic analytical balance at the outlet. Permeability and dimensionless fracture conductivity under various operating conditions were calculated using Darcy's law based on the recorded differential pressure and flow rate data.

Using dynamic fracture conductivity F_D measured across varying closure stresses in the coupled experimental setup, and incorporating the Cinco-Ley equivalent wellbore radius model for finite-conductivity vertical fractures [33], a quantitative workflow bridging laboratory tests to field productivity was established to evaluate the long-term production potential of phase-change self-propped fractures.

Dimensionless fracture conductivity F_D:

$$F_D = \frac{k_f w_f}{k x_f} \tag{1}$$

The Cinco-Ley equivalent wellbore radius method was applied to determine fractured well productivity; the intermediate variable u, empirical coefficient F, and equivalent wellbore radius are expressed as follows:

$$u = \ln(F_D) \tag{2}$$

$$F = \frac{1.65 - 0.328u + 0.116u^2}{1 + 0.18\mathrm{u} + 0.064u^2 + 0.005u^3} \tag{3}$$

$$r_e' = \frac{x_f}{2} e^{-F} \tag{4}$$

Fractured well productivity Q:

$$Q = \frac{2\pi kH(P_i - P_w)}{\mu_o \beta_o \ln(\frac{r_e}{\frac{x_f}{2}e^{-F}})} \quad (5)$$

where: k_f is fracture permeability, mD; w_f is fracture width, m; k is reservoir matrix permeability, mD; x_f is fracture half-length, m; H is reservoir thickness, m; P_i is reservoir pressure, MPa; P_w is bottomhole flowing pressure, MPa; is crude oil viscosity, mPa穘; is crude oil formation volume factor; r_e is drainage radius, m; and is equivalent wellbore radius, m.

1.3 Experimental Design

The viscosities of fracturing fluids vary significantly across temperatures. Fig. xx illustrates the comparative viscosity profiles of 1? and 2? broken slickwater fracturing fluid versus the phase-change self-propping fracturing fluid between 20 癈 and 80 癈. Experimental results demonstrate that maintaining an appropriate fluid viscosity mitigates fluid invasion into the formation, thereby effectively curbing leak-off.

Core plugs spanning multiple permeability classes were utilized to simulate diverse formation conditions and evaluate the impact of different fracturing fluid systems on productivity. A total of 18 core plugs categorized into low-, medium-, and high-permeability classes were prepared and allocated into six experimental groups (A through F). The six core groups were subjected to formation damage induced by: phase-change self-propping fluid carrying 1‰ slickwater, phase-change self-propping fluid carrying 2‰ slickwater, and pure broken slickwater systems at concentrations of 1‰, 2‰, 6‰ and 8‰, respectively. Initial permeability, porosity, and post-damage properties of all core plugs are summarized in Table 1.

Table 1 Basic parameters of cores

Core Number	Porosity/%	10PV/mL	Initial Permeability/mD	Final Permeability/mD
A1	5.82	13.57	20.2	17.5
A2	5.24	12.33	1.9	1.6
A3	4.84	12.18	0.12	0.09
B1	5.76	13.24	15.4	12.6
B2	5.21	12.98	1.5	1.2
B3	4.91	12.72	0.21	0.17
C1	5.65	13.41	12.1	8.5
C2	5.13	12.48	1.5	1.1
C3	4.88	11.91	0.16	0.08
D1	5.68	12.93	12.59	9.16
D2	5.22	12.73	2.46	2.04

D3	4.96	12.48	0.11	0.06
E1	5.76	12.84	18.24	4.85
E2	5.18	12.11	2.68	1.07
E3	4.75	11.94	0.34	0.04
F1	5.82	12.74	14.28	2.81
F2	4.92	12.08	1.48	0.29
F3	4.51	11.82	0.19	0.02

2 Experimental Procedure and Analysis

2.1 Experimental Process

2.1.1 Core Damage Induced by Broken Slickwater Systems with Varying Viscosities

The figure below shows the core end faces following damage by the 1? broken slickwater. Dense filter cakes formed during flooding significantly impaired core permeability, thereby heavily restricting productivity.



(a) (b) (c)

Fig. 3 End faces of core plugs damaged by 1‰ broken slickwater with a permeability range of (a) 0.1 − 1 mD, (b) 1 − 10 mD, and (c) 10 − 20 mD, respectively.

As depicted in Fig. 3 for the three permeability ranges, flooding with 1‰ broken slickwater resulted in dense, pronounced filter cakes across all end faces. These cakes severely compromised core permeability and impaired hydrocarbon flow.

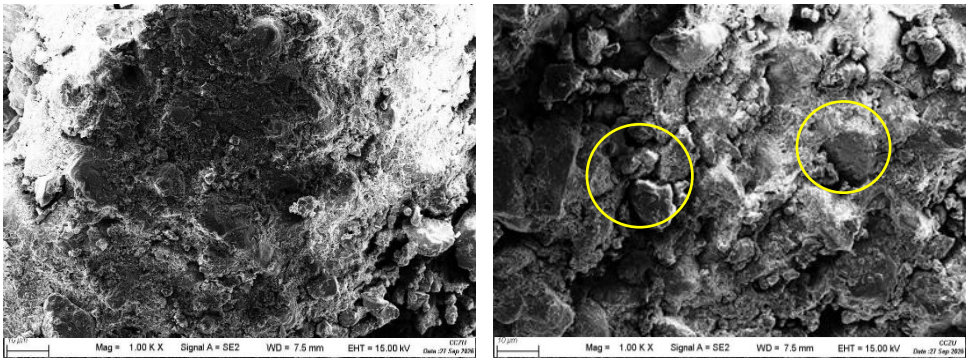

(a) (b)

Fig. 4 SEM micrographs of core end faces before (a) and after (b) damage by 1‰ broken slickwater.

SEM micrographs of the core end faces before and after damage reveal substantial polymer retention and residue accumulation from the broken slickwater, forming a covering layer or a filter-cake-like barrier of a certain thickness. This residue plugged pore throats, degraded their connectivity, and narrowed hydrocarbon percolation channels, ultimately penalizing hydrocarbon production.

Experimental results indicate that the 1‰ and 2‰ broken slickwater formulations exhibit similar viscosity, yielding filter cakes on the core end faces with no discernible morphological differences. The phase-change self-propping fluid generates uniformly sized solid proppant grains in situ, effectively sustaining fracture conductivity; in contrast, broken slickwater fails to provide propping capability, offering no structural support to enhance hydrocarbon recovery.



(a) (b) (c)

Fig. 5 End faces of core plugs damaged by 2‰ broken slickwater with a permeability range of (a) 0.1 − 1 mD, (b) 1 − 10 mD, and (c) 10 − 20 mD, respectively.

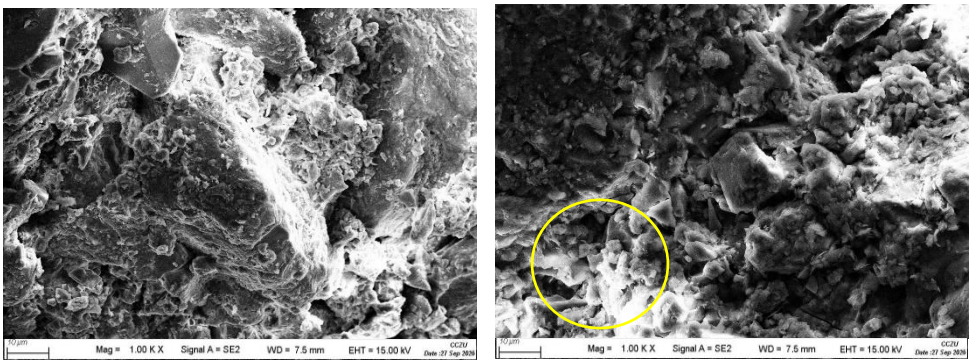

(a) (b)

Fig. 6 SEM micrographs of core end faces before (a) and after (b) damage by 2‰ broken slickwater.

Although the 2‰ broken slickwater possesses a marginally higher viscosity than the 1‰ formulation, experimental results indicate that its permeability impairment was unexpectedly lower. The higher viscosity of the 2‰ formulation increases resistance to flow into the rock matrix compared with

lower-viscosity fluids. This limits both the depth and volume of fluid invasion, reducing damage to internal pore throats and resulting in less overall formation damage.

The figures below present the core end faces damaged by 6‰ broken slickwater. The resulting filter cakes were markedly thicker and denser than those produced by the 1‰ and 2‰ systems, causing substantially greater permeability degradation and productivity loss.



(a) (b) (c)

Fig. 7 End faces of core plugs damaged by 6‰ broken slickwater with a permeability range of (a) 0.1 − 1 mD, (b) 1 − 10 mD, and (c) 10 − 20 mD, respectively.

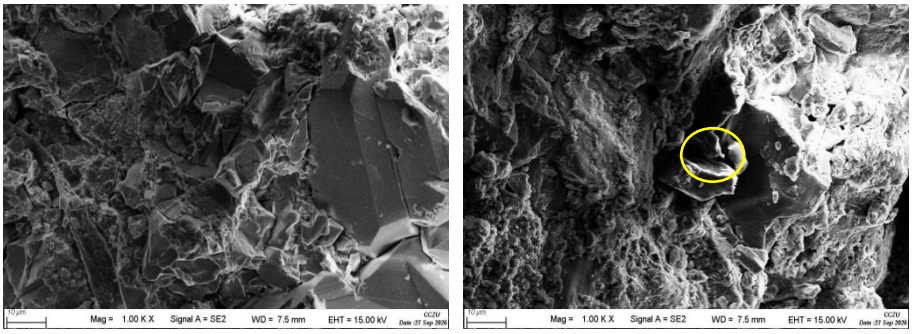

(a) (b)

Fig. 8 SEM micrographs of core end faces before (a) and after (b) damage by 6‰ broken slickwater.

The figures below display the core end faces damaged by the 8? broken slickwater. Owing to its highest viscosity, this system exhibited the most severe residue retention on the rock face, generating an impermeable cake that caused the most catastrophic permeability reduction and productivity impairment.



(a) (b) (c)

Fig. 9 End faces of core plugs damaged by 8? broken slickwater with a permeability range of (a) 0.1–1 mD, (b) 1–10 mD, and (c) 10–20 mD, respectively.

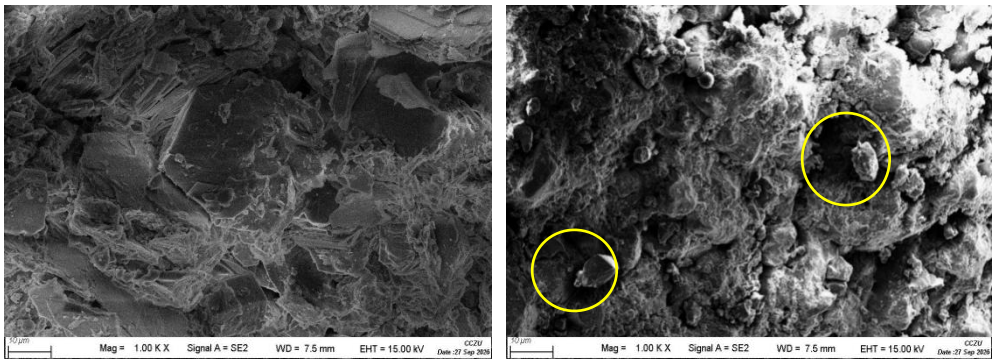

(a) (b)

Fig. 10 SEM micrographs of core end faces before (a) and after (b) damage by 8? broken slickwater.

2.1.2 Core Damage Induced by Phase-Change Self-Propping Fluid Combined with Broken Slickwater of Varying Viscosities

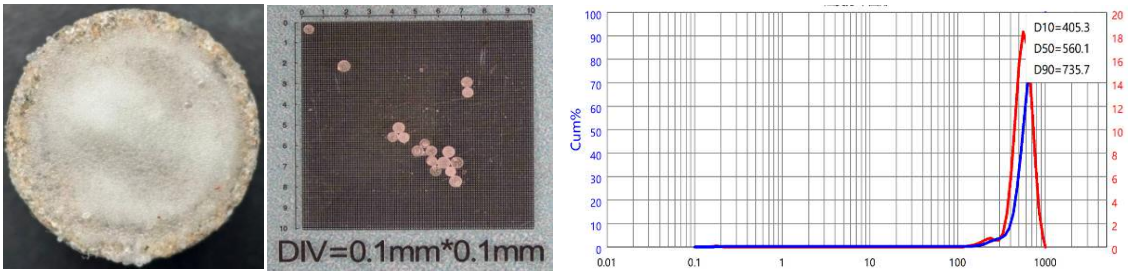

(a)

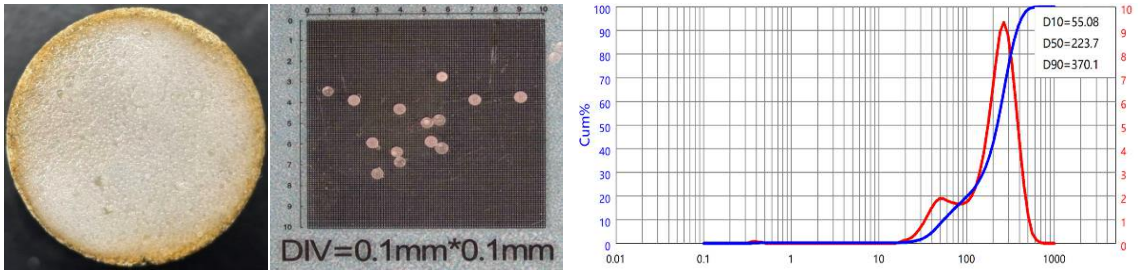

(b)

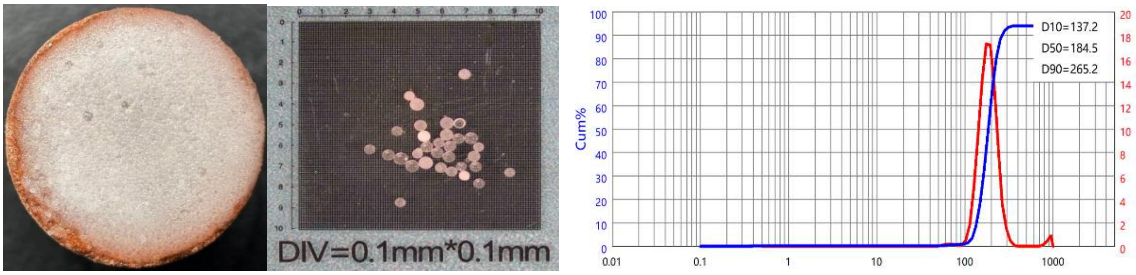

(c)

Fig. 11 Proppant placement morphology and grain size distribution following damage by the phase-change self-propping fluid carrying 1% broken slickwater: (a) 0.1–1 mD, (b) 1–10 mD, and (c) 10–20 mD core plugs.

The phase-change self-propping fracturing fluid generated proppant particles in situ across the core end face. Grain size analysis confirmed their high uniformity, and the resulting proppant pack exhibited robust propping performance under stress in the conductivity cell.

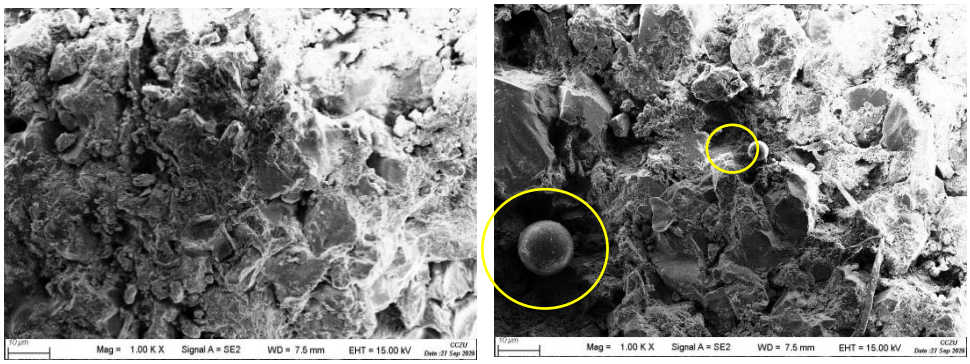

(a) (b)

Fig. 12 SEM micrographs of core end faces before (a) and after (b) damage by the phase-change self-propping fluid combined with 1‰ broken slickwater

As observed in the micrographs, the phase-change fluid solidifies into spherical particles on the core end face, substantially mitigating flow path constriction.

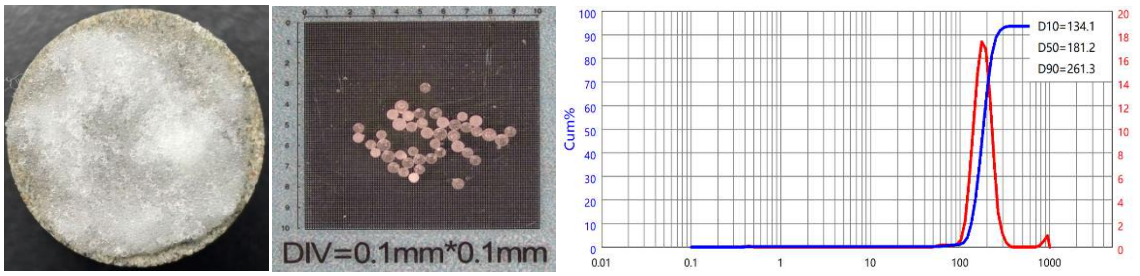

(a)

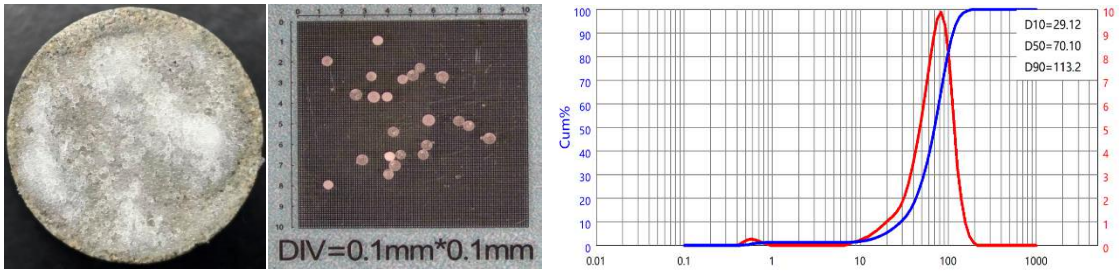

(b)

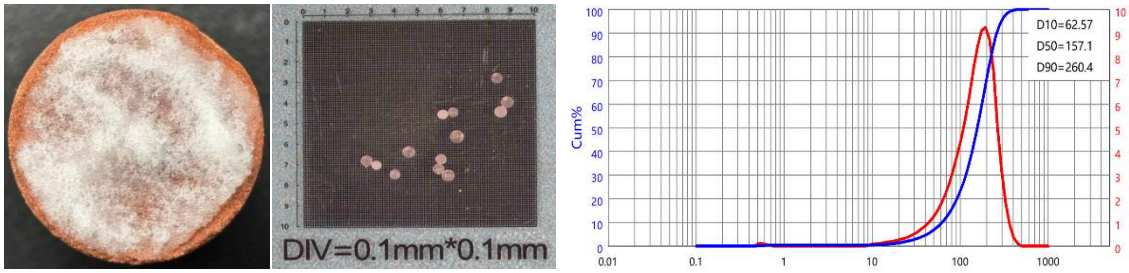

(c)

Fig. 13 Proppant placement morphology and grain size distribution following damage by the phase-change self-propping fluid combined with 2% broken slickwater: (a) 0.1–1 mD, (b) 1–10 mD, and (c) 10–20 mD core plugs.

The use of different carrier fluids to formulate the phase-change self-propping fracturing fluid yielded minimal variation in their effects on the core end faces; no significant differences were observed in solid deposition, filter cake morphology, or damage characteristics. Furthermore, all formulations underwent a reliable phase transition across different carrier fluids, yielding proppant grains with uniform size and consistent distribution. This indicates that carrier fluids exert negligible influence on particle nucleation or rock-face impairment, demonstrating the high operational robustness and broad compatibility of the system.

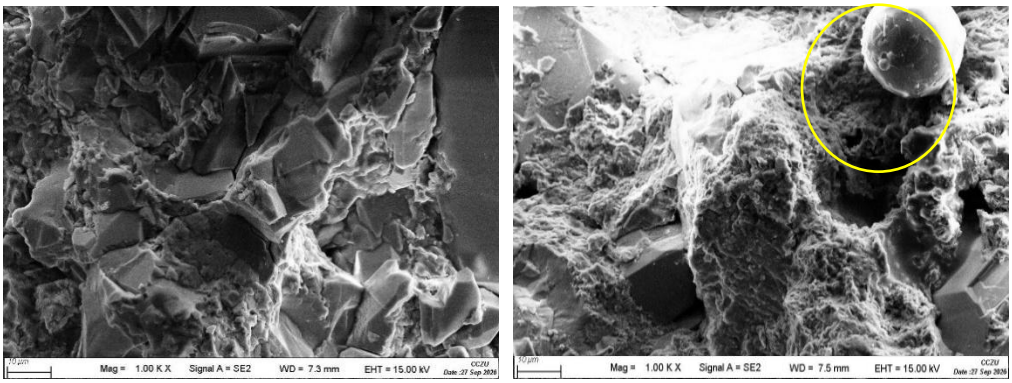

(a) (b)

Fig. 14 SEM micrographs of core end faces before (a) and after (b) damage by the phase-change self-propping fluid combined with 2% broken slickwater.

2.1.3 Core Damage and Proppant Testing

The phase-change self-propping fracturing fluid induced minimal matrix damage; in contrast, low-viscosity broken slickwater systems caused substantially greater damage.

Table 2 Summary of core damage

Core Number	Final Permeability/mD	Damage Rate/%
A1	17.5	13.4
A2	1.6	15.8
A3	0.09	25.0
B1	12.6	18.2
B2	1.2	20.0
B3	0.17	19.1
C1	8.5	29.8
C2	1.1	26.7
C3	0.08	50.0
D1	9.16	27.2
D2	2.04	17.1
D3	0.06	45.5
E1	4.85	73.4
E2	1.07	60.1
E3	0.04	88.2
F1	2.81	80.3
F2	0.29	80.4
F3	0.02	89.5

Under a closure stress of 50 MPa, the in-situ generated solid phase underwent only minor local cracking without catastrophic grain crushing or structural collapse. This demonstrates excellent structural

integrity and compressive stability under high stress, thereby causing only a minor reduction in fracture conductivity.

Proppant Type	Bulk Density（g/cm^3）	Apparent Density（g/cm^3）
20-40Mesh Phase-Change Solid Phase	0.44	1.08
20-40Mesh Quartz Sand	1.55	2.54
20-40Mesh Ceramsite	1.78	2.81

Table 3 Bulk density and apparent density of tested proppants

Marked differences in bulk density and apparent density were observed among the three proppants, which directly govern their transport behavior in carrier fluids of varying viscosities. Owing to its ultra-low density and high compressive strength, the phase-change solid phase can be placed deep into extended fracture networks, effectively propping distal fractures.

The figures below show the microscopic morphology of the phase-change proppant pack retrieved from the conductivity cell under various closure stresses, revealing only minor local crushing.

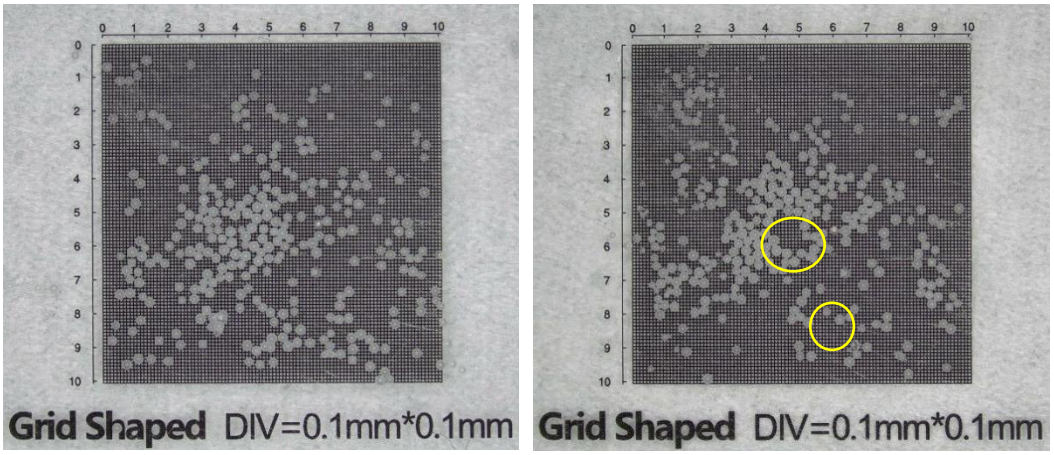

(a) **(b)**

Fig. 16 Microscopic comparison of the phase-change solid phase before and after loading: (a) before loading and (b) deformation after loading.

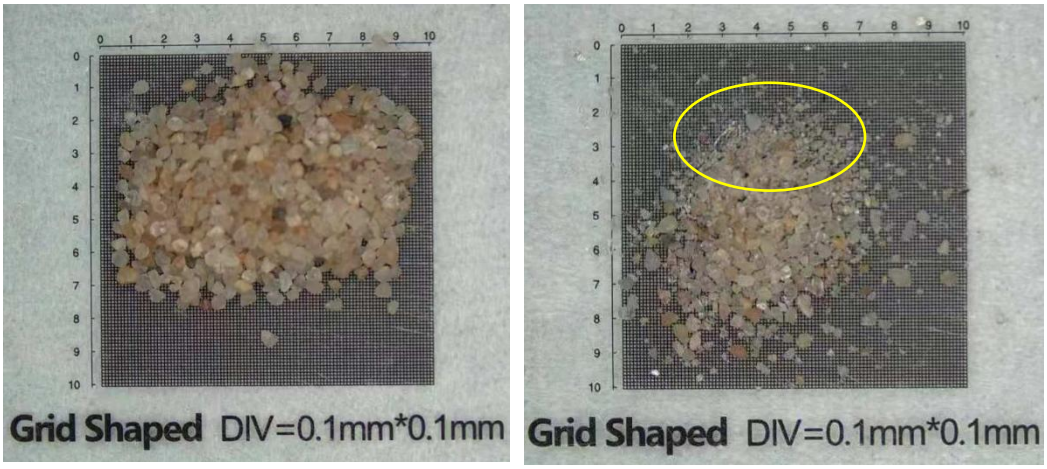

(a) (b)

Fig. 17 Microscopic comparison of quartz sand proppant before and after loading: (a) before loading and (b) crushing after loading.

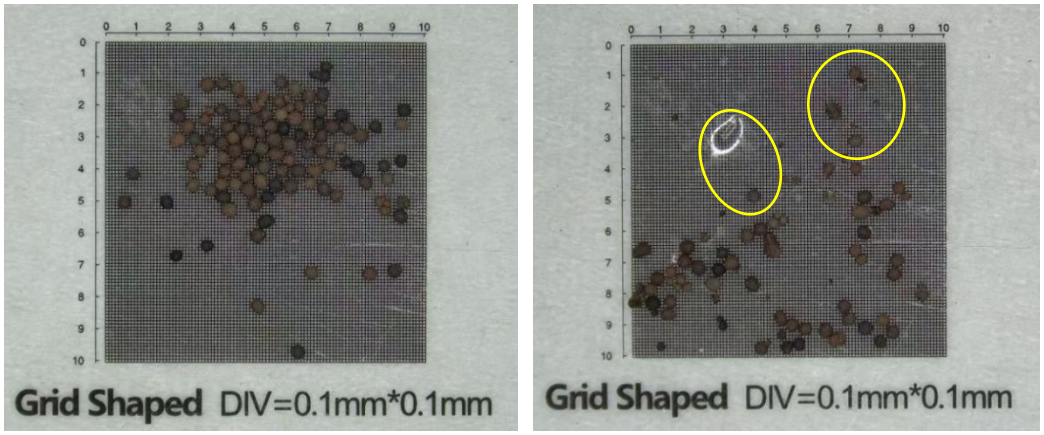

(a) (b)

Fig. 18 Microscopic comparison of ceramic proppant before (a) and after (b) loading

After being subjected to a closure stress of 50 MPa, the 20 – 40 mesh ceramic proppant exhibited a high crush rate, leading to poor fracture propping performance.

Across cores of three permeability classes, six treatment scenarios spanning four fracturing fluid systems were comparatively tested: (1) 1‰ broken slickwater with 20 – 40 mesh quartz sand, (2) 2‰ broken slickwater with 20 – 40 mesh quartz sand, (3) 6‰ broken slickwater with 20 – 40 mesh ceramic proppant, (4) 8 ‰ broken slickwater with 20 – 40 mesh ceramic proppant, (5) phase-change self-propping fluid flushed with 1‰ broken slickwater generating 20 – 40 mesh particles, and (6) phase-change self-propping fluid flushed with 2 ‰ broken slickwater generating 20 – 40 mesh particles. The proppant areal concentration was maintained at 3 kg/m² . Once the specified closure stress was applied and steady-state effluent flow was established, flow rates were logged and incorporated into the calculation equation to determine the productivity. Under varying closure stresses, the calculated productivity values across different core types are presented as follows. In the simulation model, k is matrix permeability, mD; x_f is fracture half-length, set to 0.15 m based on the cell dimensions; H is reservoir thickness, set to 0.05 m with reference to the core length; P_i is reservoir pressure, simulated by closure pressure applied, MPa; P_w is bottomhole flowing pressure, simulated by closure pressure applied, MPa; is crude oil viscosity, taken as 0.81 mPa稬 based on diesel at 80 癈; is the oil formation volume factor, set to 1.05 for diesel; r_e is drainage radius, m; and is equivalent wellbore radius, m.

Table 4 Productivity using different fracturing fluid systems across varying closure stresses

Closure Pressure(MPa)	Fracturing Fluid Type	k (mD)	w_f (mm)	F（um²*cm）	Equivalent Wellbore Diameter（m）	Q (m^3/d)
20	Phase-Change Self-Propping	0.09	4.8	5.19	0.047	0.24

30	+ 1‰ Slickwater		4.7	4.19	0.046	0.23
40	(Phase-Change Solid Phase)		4.5	2.09	0.045	0.22
50			4.4	1.47	0.043	0.21
20	Phase-Change Self-Propping		4.5	5.84	0.046	0.37
30	+ 2‰ Slickwater	0.17	4.3	4.48	0.045	0.35
40	(Phase-Change Solid Phase)		4.2	2.94	0.044	0.34
50			4.1	1.24	0.043	0.32
20			4.2	4.82	0.039	0.22
30	1‰ Gel-Breaking Slickwater	0.08	4.1	1.78	0.026	0.19
40	(Quartz Sand)		4.0	0.62	0.025	0.17
50			3.9	0.51	0.022	0.16
20			4.3	4.51	0.034	0.24
30	2‰ Gel-Breaking Slickwater	0.06	4.2	1.47	0.032	0.23
40	(Quartz Sand)		4.1	0.55	0.029	0.23
50			4.1	0.41	0.025	0.22
20			3.4	4.88	0.042	0.23
30	6‰ Gel-Breaking Slickwater	0.04	3.3	2.84	0.041	0.22
40	(Ceramsite)		3.2	1.24	0.039	0.19
50			3.1	0.67	0.037	0.17
20			3.3	4.76	0.038	0.14
30	8‰ Gel-Breaking Slickwater	0.02	3.2	3.08	0.035	0.13
40	(Ceramsite)		3.1	1.18	0.032	0.13
50			3.1	0.58	0.029	0.12

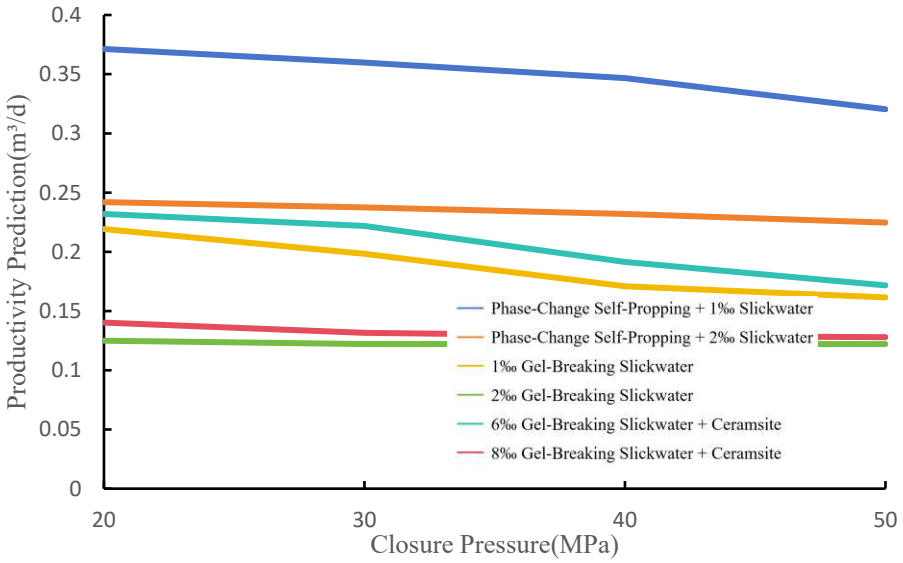

Fig. 19 Predicted productivity using three fracturing fluid systems in 0.1 – 1 mD cores

In 0.1 – 1 mD cores, the phase-change fluid’s high viscosity limited its invasion into the core, while its phase transition led to the formation of uniformly distributed proppant particles on the core end face

with little obstruction to flow. By contrast, the 6? and 8? broken slickwater fluids formed dense filter cakes on the rock end face, reducing matrix permeability and impairing productivity.

Table 5 Productivity using different fracturing fluid systems across varying closure stresses

Closure Pressure(MPa)	Fracturing Fluid Type	k (mD)	w_f (mm)	F（um²*cm）	Equivalent Wellbore Diameter（m）	Q (m^3/d)
20	Phase-Change Self-Propping + 1‰ Slickwater (Phase-Change Solid Phase)	1.6	5.4	4.18	0.071	2.23
30			5.3	3.25	0.065	2.16
40			5.1	2.91	0.053	2.09
50			4.9	2.46	0.043	2.06
20	Phase-Change Self-Propping + 2‰ Slickwater (Phase-Change Solid Phase)	1.2	5.4	4.94	0.058	2.62
30			5.3	4.11	0.049	2.53
40			5.2	3.81	0.042	2.46
50			5.0	3.28	0.039	2.41
20	1‰ Gel-Breaking Slickwater (Quartz Sand)	1.1	4.4	3.89	0.049	2.15
30			4.2	3.59	0.047	2.10
40			4.1	2.85	0.042	2.07
50			4.0	2.18	0.034	2.00
20	2‰ Gel-Breaking Slickwater (Quartz Sand)	2.04	4.3	3.76	0.043	1.98
30			4.2	3.41	0.041	1.89
40			4.1	2.71	0.037	1.79
50			3.9	1.94	0.036	1.65
20	6‰ Gel-Breaking Slickwater (Ceramsite)	1.07	3.8	3.41	0.039	2.21
30			3.7	2.19	0.034	2.17
40			3.6	1.84	0.029	2.11
50			3.5	1.26	0.024	2.02
20	8‰ Gel-Breaking Slickwater (Ceramsite)	0.29	3.9	3.59	0.031	2.02
30			3.7	2.51	0.028	1.92
40			3.5	1.86	0.022	1.81
50			3.4	1.48	0.019	1.71

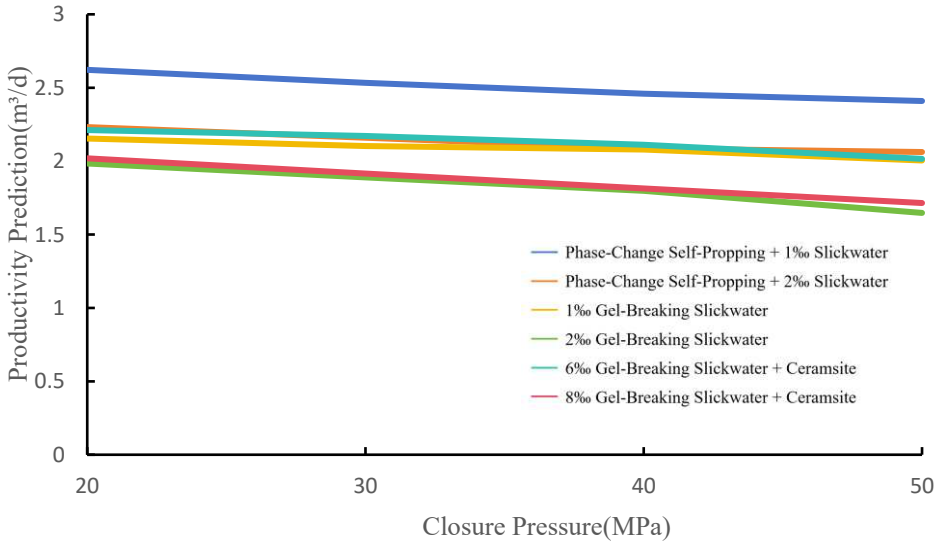

Fig. 20 Predicted productivity using three fracturing fluid systems in 1 – 10 mD cores

In cores within the 1 – 10 mD permeability range, the cores subjected to damage by the phase-change self-propping fracturing fluid exhibited marked advantages over those damaged by broken slickwater. Their productivity tended to stabilize across different closure pressures, ensuring both stable propping and steady productivity under various closure stresses.

Table 6 Productivity using different fracturing fluid systems across varying closure stresses

Closure Pressure(MPa)	Fracturing Fluid Type	k (mD)	w_f (mm)	F（um²*cm）	Equivalent Wellbore Diameter（m）	Q (m³/d)
20	Phase-Change Self-Propping + 1‰ Slickwater (Phase-Change Solid Phase)	17.5	4.8	8.85	0.084	14.19
30			4.7	7.02	0.081	13.71
40			4.5	5.05	0.078	13.26
50			4.4	4.87	0.071	12.48
20	Phase-Change Self-Propping + 2‰ Slickwater (Phase-Change Solid Phase)	12.6	4.6	7.05	0.079	17.89
30			4.5	6.15	0.074	17.31
40			4.3	4.91	0.064	16.75
50			4.1	3.56	0.062	15.78
20	1‰ Gel-Breaking Slickwater (Quartz Sand)	8.5	4.2	6.86	0.068	13.06
30			4.1	4.01	0.059	12.82
40			3.9	3.68	0.051	12.09
50			3.8	2.94	0.048	11.92
20	2‰ Gel-Breaking Slickwater (Quartz Sand)	9.16	4.3	6.48	0.066	11.95
30			4.2	3.84	0.058	11.14
40			4.1	3.41	0.048	11.03
50			4.0	2.47	0.043	10.73
20	6‰ Gel-Breaking Slickwater	4.85	3.8	7.48	0.059	13.71

30	(Ceramsite)		3.7	5.18	0.054	13.31
40			3.5	4.84	0.042	12.82
50			3.4	3.68	0.039	11.16
20			3.8	6.92	0.049	12.16
30	8‰ Gel-Breaking Slickwater	2.81	3.7	6.18	0.042	12.06
40	(Ceramsite)		3.6	5.19	0.038	11.82
50			3.4	3.18	0.033	11.12

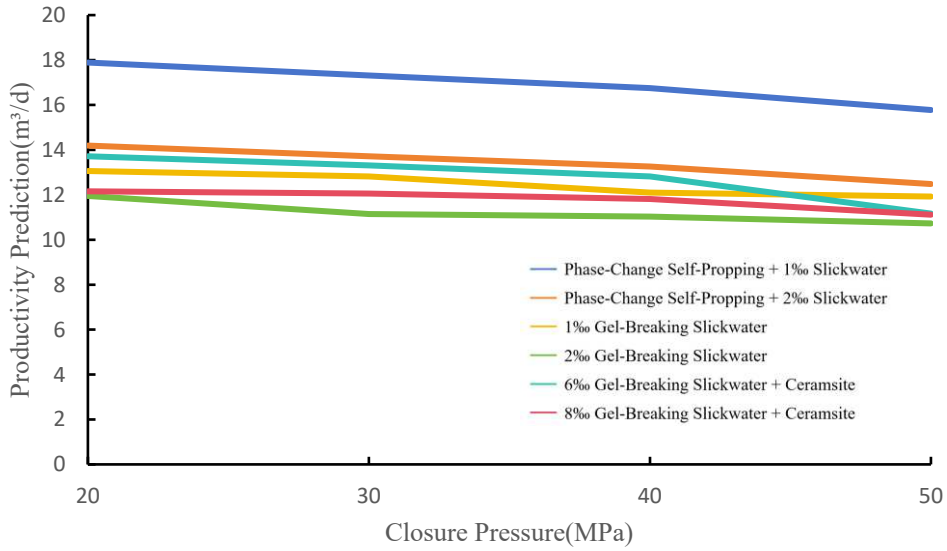

Fig. 21 Predicted productivity using three fracturing fluid systems in 10 − 20 mD cores

Taken together, the three figures show that the phase-change self-propping fracturing fluid performs consistently across the tested operating conditions and outperforms broken slickwater fracturing fluids in reservoir fractured production. In high-permeability cores, the best stimulation results were obtained when the phase-change fluid was combined with 1‰ slickwater. In low-permeability reservoirs, the phase-change self-propping fracturing fluid mixed with 1? viscosity slickwater fracturing fluid yields the best reservoir stimulation effect. Because low-viscosity slickwater causes minimal matrix impairment, it substantially enhances overall fracturing efficiency.

2.2 Analysis of Experimental Results

The experimental findings demonstrate that the phase-change self-propping fluid combined with 1? broken slickwater delivers significantly higher post-fracturing productivity than conventional slickwater carrying quartz sand or ceramic proppant. Conventional broken slickwater readily generates impermeable filter cakes across the core end face, constricting flow channels and impeding hydrocarbon drainage into propped fractures. In contrast, the phase-change fluid forms permeable solid proppant packs in situ on the rock end face, establishing high-conductivity percolation pathways within the fracture network. Consequently, this in-situ propping mechanism can effectively reduce formation damage while sustaining high-flow conduit connectivity.

3 Field Application

3.1 Field Data

To validate the laboratory findings under operational conditions, Well D45-X in the Daqing Oilfield was selected as a pilot field for refracturing stimulation to increase productivity. Well D45-X was brought on stream in May 2009, targeting the Chang 4+5 formation with a single 4-m perforated interval and an initial test production of 6.9 m^3 /d. Two water injection wells are provided for hydraulic fracturing of the same formation segment. During its first three years of production, the well exhibited stable performance, averaging 1.5 m^3 /d of total fluid, 1.0 t/d of oil, and a water cut of 15%. In February 2013, production declined to 0.6 m^3 /d of fluid and 0.4 t/d of oil, with the water cut rising to ~30%; prolonged low-efficiency production persisted despite repeated adjustments of water injection rates on site. In January 2025, a surfactant unblocking treatment yielded a modest recovery, providing a daily incremental oil production of 0.2 t/d and a cumulative incremental gain of 40 t through late May. Prior to refracturing, production stood at 0.9 m^3 /d of fluid and 0.5 t/d of oil, with a water cut of 33.3%. The well controls 2.07×10^4t of geological reserves, with cumulative oil production of 2,946 t (recovery factor of 14.24%) and remaining recoverable reserves of 17,752.32 t.

Table 7 Comparison of operational parameters between initial fracturing and refracturing

Fracturing Frequency	Sand Volume（m^3）	Fracturing Fluid Type	Treatment Fluid Volume（m^3）	Treatment Pump Rate（m^3/min）	Average Daily Production（t）
Primary Fracturing	30 m^3Quartz Sand	Gel-Breaking Slickwater Fracturing Fluid	/	1.6	0.4
Secondary Fracturing	8.4 m^3Solid Phase+25.35 m^3Quartz Sand	Phase-Change Self-Propping Fracturing Fluid	640.90	0.5-2.0	2

Following the initial fracturing treatment, well productivity remained suboptimal at approximately 0.4 t/d of oil, necessitating refracturing. The refracturing design adopted a hybrid strategy: deploying the phase-change self-propping fluid across the complex fracture network, while placing in-situ generated solid proppant packs along intermediate fracture sections. Refracturing was executed using the phase-change self-propping fluid, resulting in continuous incremental oil recovery since pumping in September 2025.

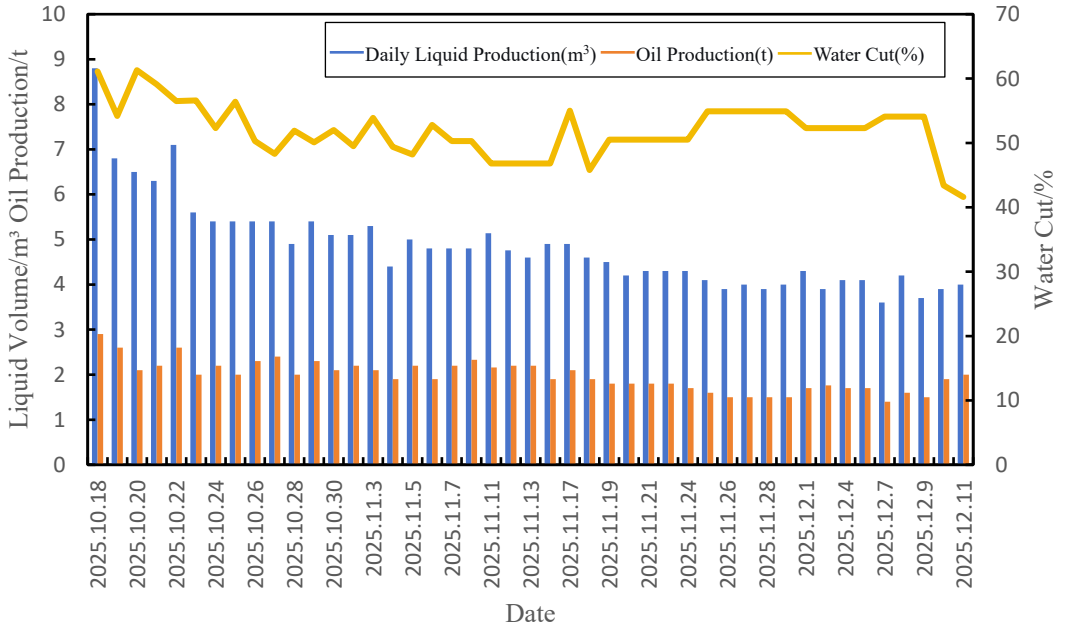

Fig. 22 Post-refracturing production performance

Following refracturing, daily oil production stabilized at 2–3 t/d. The use of the phase-change self-propping fluid as the primary carrying medium to generate and place solid proppants in situ successfully validated the laboratory design concept, demonstrating practical guidance for field-scale application.



Fig. 23 Field operational layout for refracturing

Utilizing a self-developed, skid-mounted pumping unit, the high-viscosity self-propping fracturing fluid and conditioning agents were injected into the wellbore. Subjected to wellbore shear, the fluid dispersed into uniform droplets; upon entering the target reservoir, formation temperature triggered in-situ phase transition and solidification into high-strength proppant packs. This mechanism effectively propped the near-wellbore, intermediate, and distal fracture regions, achieving superior full-network conductivity.

3.2 Field Experiment Results

Coupled core flooding and fracture conductivity testing under simulated closure stresses confirms that fractures stimulated by the phase-change self-propping fluid achieve substantially higher conductivity, larger effective apertures, and expanded drainage areas, thereby markedly enhancing matrix – fracture flow capacity. Furthermore, the fluid and in-situ generated proppants induce minimal matrix permeability impairment, accompanied by negligible fracture-face skin, minimal proppant embedment and crushing, and low residue retention. These features deliver high permeability recovery and conductivity retention, demonstrating pronounced low-damage characteristics. Over a 118-day post-fracturing production monitoring period, Well D45-X achieved a 3.75- to 5.5-fold increase in daily oil production over pre-treatment baselines and sustained steady output, demonstrating the reliability of the productivity predictions in the coupled experiment. Consequently, this fracturing system and technique can achieve highly effective stimulation and superior productivity while mitigating formation damage, providing robust experimental and operational foundations for parameter optimization and production forecasting in similar reservoirs.

4 Conclusions

This study investigated the comparative impacts of a phase-change self-propping fracturing fluid versus conventional broken slickwater systems of varying viscosities on post-stimulation productivity. The results demonstrate that the phase-change fluid delivers superior stimulation performance throughout production. Field trials further confirm that this system induces minimal reservoir damage, and the in-situ solidified particles reliably prop complex fracture networks to facilitate hydrocarbon recovery.

(1) Across reservoirs with a permeability range of 0.1–20 mD, the phase-change self-propping fluid combined with 1% broken slickwater generated solid proppant particles in situ. Laboratory results predicted productivity 1.3–1.6 times that of conventional proppant-laden broken slickwater systems, while field operations showed an approximately fourfold increase in production.

(2) SEM observations demonstrate that the phase-change self-propping fluid causes substantially less matrix damage than broken slickwater systems. Attributed to its high viscosity, the fluid exhibits low leak-off and minimal residue deposition, thereby mitigating formation damage and offering superior environmental compatibility.

(3) Productivity under the phase-change self-propping fracturing system declines at a markedly slower rate with increasing closure stress than conventional systems, demonstrating excellent stress insensitivity and sustained conductivity under high in-situ closure stresses.

In summary, the phase-change self-propping fracturing fluid delivers significant advantages, including minimal formation damage and sustained high productivity. This study provides reference for productivity prediction across diverse reservoir types.

Funding Declaration:
This research received no specific grant from any funding agency in the public, commercial, or not-for-profit sectors.

Data Availability Declaration:
The datasets generated during and/or analysed during the current study are available from the corresponding author on reasonable request.

Competing Interest Declaration:
The authors declare that they have no known competing financial interests or personal relationships that could have appeared to influence the work reported in this paper.

Reference

[1] An Qiyi, Zhang Qingsong, Li Xianghui, Yu Hao, Yin Zhanchao, Zhang Xiao. Accounting for dynamic alteration effect of SC-CO2 to assess role of pore structure on rock strength: A comparative study[J]. Energy.2022

[2] Zhang Xueping, Liu Youquan, Liu Yuzhou, Zhong Chuanrong. Influencing Factors and Application of Spontaneous Imbibition of Fracturing Fluids in Tight Sandstone Gas Reservoir.[J]. ACS omega.2022

[3] Liu J, Qu X, Wang J, et al. Investigating the Influencing Factors of Imbibition of Fracturing Fluids in Tight Reservoirs[J]. Processes, 2024,12(1):236.

[4] Liu Chengting, Hu Chuanfeng, Wang Zhigang, etc. Research on the Proppant Distribution in Fractures from Channel Fracturing[J]. Henan Science, 2024.

[5] Weijia Cao, Kun Xie, Xiangguo Lu, Qing Chen, Zhongyuan Tian, Wei Lin. Self-suspending proppant manufacturing method and its property evaluation[J]. Journal of Petroleum Science and Engineering.2020

[6] Huang Jing, Liu Yuan, Zhang Wangqing. Research Progress of Polyacrylamide-based Polymer Drag Reducer[J]. Ion Exchange and Adsorption, 2025,41(3):240-251.

[7] Zhu Ruibin, Liu Guohua, Zhao Liqiang, Experimental Study on Filtration Characteristics of Temperature-controlled Chemical Fracturing Fluid[J]. Science Technology and Industry, 2024,24(22):334-339.

[8] Yu Donghe, Chen Weiyu, Liu Guohua, etc. Preparation and Performance Evaluation of Supramolecular Phase Change Fracturing Fluid with Thermal Stimuli-response[J]. Oilfield Chemistry, 2021,38(2):223-229.

[9] He Li, Qingyi Guo, Meng Liu, Jiexin Lu, Yidu Hong, Ting Liu, Zheng Wang. Petrophysical characterization of coal subjected to cyclic N-methylpyrrolidone treatment based on two-dimensional NMR T1-T2[J]. .Fuel.2024

[10] Jia Chengzao, Jiang Lin, Zhao Wen. Tight oil and gas in Whole Petroleum System: accumulation mechanism, enrichment regularity, and resource prospect[J]. Acta Petrolei Sinica, 2025.

[11] Zhu Yue, Wu Shunwei, Deng Yusen, etc. Pore Throat Structures and Fluid Occurrences of Reservoirs in Fengcheng Formation, Mahu Sag[J], Xinjiang Petroleum Geology, 2024.

[12] Zhang Yang, Zhang Shiling. Research Progress of Controllable Breaking Technology for Ultra-High-Temperature Fracturing Fluids[J]. Xinjiang Oil & Gas, 2026,22(3):104-111.

[13] Guang Xinjun, Wang Minsheng, etc. Proppants for Fracturing Fluids: New Progress Made and Direction of Future Development[J]. Drilling Fluid&Completion Fluid, 2021.

[14] Cai Xidong, Zhang Na, Ge Fangrong. Supramolecular Surfactant Fracturing Fluid Suitable for Unconventional Oil and Gas Reservoirs[J].Oilfield Chemistry, 2025,42(2):236-243.

[15] Tong Shaokai, Yue Yanfang, Zhang Hongzhong, etc. Study on fracturing technology of temperature-controlled expandable proppants in unconventional reservoirs: 2025（IPPTC）[C], Beijing, China, 2025.

[16] Ren Guirong, Liu Yuan, Pan Baofeng, etc. Research and Application of Low-temperature Breakers for Polymer Fracturing Fluids[J]. Sino-Global Energy,2025,30(12):48-53.

[17] Pei, Y.; Tang, A.; Zhu, J.; Zhang, L.; Shan, X.; Tang, W.; Song, F. Experimental Study on the Impact of Phase-Change Self-Propping Fracturing Fluid on Reservoir Invasion Damage. Appl. Sci. 2026, 16, 1190. https://doi.org/10.3390/app16031190

[18] Chen Y, Sang Y, Guo J, et al. Liquid–Solid Phase-Change Autogenous Proppant Fracturing Fluid& Phase-Change Behavior Research and Field Application[J]. Energy & FuelsEnergy & Fuels, 2023,37(21):16333-16344.

[19] Wang Tao, Li Congni, Li Junli. Research progress and development trend of temperature and salt resistant fracturing fluid technology[J]. Applied Chemical Industre:1-11.

[20] Zhang Sanfeng, Wu Jinqiao, Lin Jin, etc. Advances in research on mechanisms and prevention and control technologies for solid-phase production in hydraulically fractured coalbed methane wells[J]. Coal Geology & Exploration, 2026,54(3):103-115.

[21] Zhao Liqiang, Zhang Nanlin, Zhang Yiming, etc. Laboratory study and field application of self-propping phase-transition fracturing technology[J]. Natural Gas Industry, 2020, 40(11): 60-67.

[22] Yutaka Ohsedo.Low-molecular-weight organogelators as functional materials for oil spill remediation[J]. Polymers for Advanced Technologies.2016

[23] Yixin Chen, Yu Sang, Jianchun Guo, Jian Yang, Weihua Chen, Botao Tang, Ruoyu Yang, Shan Yi; Liquid–Solid Phase-Change Autogenous Proppant Fracturing FluidPhase-Change Behavior Research and Field Application. *Energy Fuels* 2 November 2023; 37 (21): 16333–16344. https://doi.org/10.1021/acs.energyfuels.3c01266

[24] Xiaofeng Zhou, Qingzhao Wang, Jianguang Wei, Haoran Cheng, Bin Huang, Demiao Shang,Study on mechanism of Pre-CO2 fracturing and analysis of sensitive factors for CO2 fracturing backflow in shale oil reservoirs, International Journal of Hydrogen Energy, https://doi.org/10.1016/j.ijhydene.2025.03.001.

[25] Hu Zhifan, Yu Ying, Pei Yongmei, etc. Multi-branch re-fracturing and stimulation technology in low permeability horizontal wells with temporary plugging and diversion[J]. Oil Production Engineering, 2019,(1):50-52+98-99.

[26] Gong Yue, Cui Yueqi, Liu Chang, etc. Analysis of factors affecting productivity of volume fracturing horizontal wells in tight sandstone reservoirs[J]. Petrichemical Industry Application,2024,43(8):13-20.

[27] Fan, H. Performance forecasting of hydraulically fractured horizontal wells using dynamic-drainage-area concept with correct distance of investigation. J Petrol Explor Prod Technol 13, 1463–1473 (2023). https://doi.org/10.1007/s13202-023-01623-4

[28] Jinzhou Zhao, Xuan Pu, Yongming Li, Xianjie He, A semi-analytical mathematical model for predicting well performance of a multistage hydraulically fractured horizontal well in naturally fractured tight sandstone gas reservoir, Journal of Natural Gas Science and Engineering, https://doi.org/10.1016/j.jngse.2016.04.011.

[29] Tonglou Guo, Zuhao Kou, Yulong Zhao, Heng Wang, Yuchen Xin, Role of gas multiple transport mechanisms and fracture network heterogeneity on the performance of hydraulic fractured multiwell-pad in unconventional reservoirs, Fuel, 2023.127808.

[30] Zhao, Yl., Li, Ny., Zhang, Lh. et al. Productivity analysis of a fractured horizontal well in a shale gas reservoir based on discrete fracture network model. J Hydrodyn 31, 552–561 (2019). https://doi.org/10.1007/s42241-018-0163-x

[31] Dongxu ZHANG, Liehui ZHANG, Huiying TANG, Yulong ZHAO, Fully coupled fluid-solid productivity numerical simulation of multistage fractured horizontal well in tight oil reservoirs, Petroleum Exploration and Development, https://doi.org/10.1016/S1876-3804(22)60032-6.

[32] Ren Long, Su Yuliang, Hao Yongmao, etc. . Dynamic analysis of SRV-fractured horizontal wells in tight oil reservoirs based on stimulated patterns[J].Acta Petrolei Sinica,2015,36(10):1272-1279.

[33] Cinco-Ley, H., & Samaniego-V., F. (1981). Transient Pressure Analysis for Fractured Wells. Journal of Petroleum Technology, 33(09), 1749–1766. SPE-7490-PA. https://doi.org/10.2118/7490-PA